Optical properties of $RbMnF_3:Er^{3+}$

M. V. Iverson and W. A. Sibley
Department of Physics, Oklahoma State University, Stillwater, Oklahoma 74074
(Received 14 August 1979)

Absorption, emission, excitation, and lifetime data are presented for $RbMnF_3:Er^{3+}$. Evidence for $Mn^{2+} \rightarrow Er^{3+}$ energy transfer was found from the Er^{3+} excitation spectra and the temperature dependence of the Mn^{2+} and Er^{3+} emissions. The presence of Er^{3+} in the lattice slightly changed the temperature dependence of the Mn^{2+} lifetime. Radiative and radiationless transitions are discussed in terms of the model of Flaherty and Di Bartolo and the quantum-mechanical single-configuration coordinate model of Struck and Fonger.

I. INTRODUCTION

Over the last twenty years concentrated manganese systems such as $RbMnF_3$ and MnF_2 have been studied by a large number of investigators.[1-25] Early studies emphasized low-temperature absorption spectra[6,10] and a determination of the energy levels for the observed bands. Emission studies[3-5,7,8] revealed a strong temperature dependence of the integrated fluorescent intensity and lifetime. Since both $RbMnF_3$ and MnF_2 are antiferromagnetic below the Néel temperature (T_N), this temperature dependence of the emission was originally interpreted as being due to a local lattice distortion coupled with magnetic interaction of excited Mn^{2+} ions. Later Gooen *et al.*[8] and Green *et al.*[7] found that energy transfer was the active process with emission originating from Mn^{2+} sites perturbed by nearby impurities. An excellent review of this process has been given by Imbusch.[18] Further evidence for energy transfer was found using the system $RbMn_xMg_{1-x}F_3$ where it was demonstrated that energy transfer occurred in crystals containing more than 30-at.% Mn^{2+}.[20]

The effect of the presence of rare-earth ions on energy transfer has been investigated. Emissions from Nd^{3+} in $RbMnF_3$,[8,13] Er^{3+} in MnF_2,[23-25,16] Eu^{3+} in MnF_2,[12,14,16] and Eu^{3+} in $KMnF_3$,[21,22] have been observed and analyzed. Flaherty and Di Bartolo[24] found that in $MnF_2:Er^{3+}$ a delocalized energy was transferred nonradiatively to the erbium for subsequent emission from the $^4F_{9/2}$ and lower levels. Also it should be noted that emission has not been observed from the $^4S_{3/2}$ level of Er^{3+} in MnF_2 although its absorption energy may be found by laser excitation.[16]

In this study we examined $RbMnF_3:Er^{3+}$ and compared it to undoped $RbMnF_3$. Section II considers experimental methods, apparatus, and actual doping levels of Er^{3+}. Section III describes the observed absorption, emission, excitation, and lifetime data. In Sec. IV we discuss the fluorescent properties of $RbMnF_3:Er^{3+}$ and $MnF_2:Er^{3+}$. Radiative and radiationless relaxation are discussed in terms of the integrated intensity and lifetime model of Flaherty and Di Bartolo[24] and the quantum-mechanical single-configuration-coordinate model (QMSCC) of Struck and Fonger.[26-30]

II. EXPERIMENTAL

The crystals used in this study were obtained through the courtesy of J. J. Martin of the Oklahoma State University Crystal Growth Facility. The concentration of Er^{3+} was determined to be ~3000 ppm from mass spectroscopy and ~500 ppm from the absorption coefficients and estimated oscillator strengths.[31,32] The melt contained 1 at.% of Er.

Low temperature optical absorption spectra were obtained using a Cary-14 spectrophotometer. The samples were mounted in a CTI Cryodyne Cryocooler with a resistance heater which allowed temperature control within ±1 K from 13 to 300 K.

Since the Er^{3+} emission occurs over a wide spectral range two different fluorescent systems were used. In the first system chopped light from a 150-W xenon lamp was passed through a 0.25-m Spex Minimate Monochrometer to excite the crystals. Emission spectra were obtained using a 1-m Jarrell-Ash Monochrometer with a RCA 31034*C* photomultiplier cooled to −20 °C. Lock-in detection was used for sufficiently short lifetimes. The two infrared Er^{3+} transitions were excited using a 300-W xenon lamp and another 0.25-m Spex Minimate. The infrared emission was dispersed by a 0.5-m Bausch and Lomb Monochrometer with grating blazed at one micron and detected by either a dry ice cooled RCA 7102 photomultiplier or an Optoelectronics OTC 22-53*XX* two stage thermoelectrically cooled PbS cell. When monitoring emission from the $^4F_{9/2} \rightarrow {}^4I_{15/2}$, $^4I_{9/2} \rightarrow {}^4I_{15/2}$, and $^4I_{13/2} \rightarrow {}^4I_{15/2}$ transitions the following filters were used: Corning CS3-69, Corning CS2-64 sharp cutoff, and a Corning CS7-57. The detection systems were calibrated using

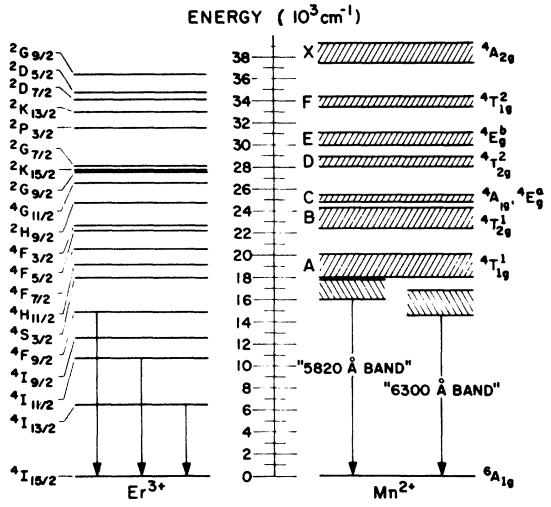

FIG. 1. Partial energy-level diagram for Mn^{2+} and Er^{3+}.

a quartz iodine lamp with spectrum traceable to the National Bureau of Standards.

Lifetime data were taken using a General Radio Strobatac Xenon flash (~5-μsec pulse) through an appropriate filter (Oriel No. 5755 interference filter for Mn^{2+} and a Corning 4-96 broadband filter to pump Mn^{2+} absorption bands for Er^{3+} emission). After preamplification the signal was fed into a Nicolet Model 1070 signal averaging system. For faster lifetimes a Biomation Model 610*B* high-speed digitizer was used to capture the signal and transmit it digitally to the Nicolet Signal Averager. The averaged results were analyzed using a PDP-11 minicomputer.

III. EXPERIMENTAL RESULTS

The energy levels for Mn^{2+} and Er^{3+} ions in $RbMnF_3$ are illustrated schematically in Fig. 1. The Er^{3+} levels are denoted by a $^{2S+1}L_J$ notation where S is the total spin, L is the total orbital angular momentum, and $J = L + S$. This notation is standard for rare earths where the crystal-field interaction is smaller than the spin-orbit interaction. Two notations are shown for Mn^{2+} absorption bands. The letters of the alphabet on the left-hand side refer to an early labeling.[6] The other set of symbols on the right is the standard crystal-field[10] group theory notation for Mn^{2+}. The superscripts $(2S+1)$ indicate the spin of the Mn^{2+} and Er^{3+} of the transitions. Actual positions of the Mn^{2+} bands were taken from the low-temperature optical absorption spectrum shown in Fig. 2. It should be noted that in addition to the strong Mn^{2+} absorption bands weaker Er^{3+} absorption bands are observed. The peak positions are summarized in Table I.

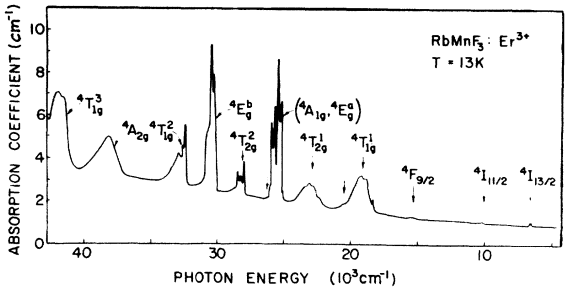

FIG. 2. Low-temperature optical absorption spectra for $RbMnF_3$:Er^{3+}. The energy of each of the Mn^{2+} and Er^{3+} absorption peaks is tabulated in Table I.

A. Manganese emission

At very low temperatures only intrinsic Mn^{2+} emission occurs in $RbMnF_3$, but by 5 K the observed 582-nm (5820 Å in Fig. 1) band is present due to energy transfer to impurity perturbed Mn^{2+} ions and subsequent emission from these sites.[7,8]

TABLE I. Energies of Mn^{2+} and Er^{3+} absorption peaks observed at 13 K in $RbMnF_3$:Er^{3+}.

Mn^{2+} Level	Mn^{2+} Energy (cm^{-1})	Er^{3+} Level	Er^{3+} Energy (cm^{-1})
$^4A_{2g}$	38 240.9		
			26 759
			26 652
	32 959.9	$^4G_{11/2}$	26 367
$^4T_{1g}$	32 626.4		26 212
	32 478		
	28 498.1		
	28 312		
$^4T_{2g}$	28 232.6	$^4F_{9/2}$	15 500
	28 011.2		
	25 994		
	25 879		
^4E_g	25 682	$^4I_{11/2}$	10 511
	25 396.8		
	25 236		
$^4A_{1g}$	25 138		
			6 596.3
			6 574.62
	23 329		
	23 095		6 563.4
			6 560
	22 321	$^4I_{13/2}$	
			6 544.5
			6 524 [a]
	19 230.7		6 513.8
	19 094		
			6 504
	18 722		
$^4T_{1g}$	18 628.9		
	18 395		
	18 292		

[a] Strongest.

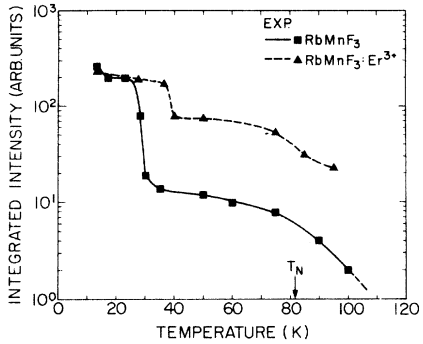

FIG. 3. Comparison of the temperature dependence of the Mn^{2+} integrated fluorescent for $RbMnF_3$ and $RbMnF_3$:Er^{3+}. The intensities shown for $RbMnF_3$ and $RbMnF_3$:Er^{3+} are unrelated.

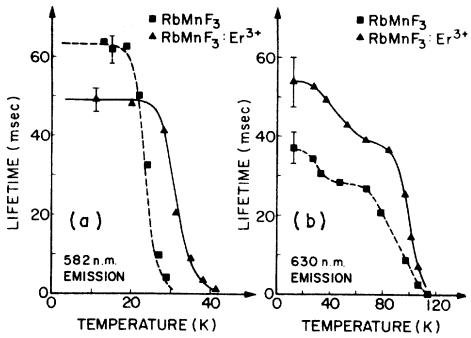

FIG. 4. (a) Comparison of the temperature dependence of the lifetime for the 582-nm (17 182-cm^{-1}) emission from nominally pure $RbMnF_3$ and Er^{3+}-doped $RbMnF_3$. The calculated temperature dependence of the lifetime using an activation process is shown by a dotted line for $RbMnF_3$ and a straight line for $RbMnF_3$:Er^{3+}. (b) Comparison of the temperature dependence of the lifetime for the 630-nm (15 873 cm^{-1}) emission from nominally pure $RbMnF_3$ and Er^{3+} doped $RbMnF_3$.

As the temperature is increased to above 40 K, energy transfer occurs from these sites to different defect-perturbed Mn^{2+} ions which have shorter lifetimes. This luminescence occurs at 630-nm (6300 Å in Fig. 1). The 630-nm band decreases in intensity until no emission is detectable above 120 K. These results are portrayed in Figs. 3 and 4 for undoped $RbMnF_3$ and $RbMnF_3$:Er^{3+}. The presence of the larger Er^{3+} ion in the lattice obviously causes some perturbation just as does the addition of the smaller Mg^{2+} for Mn^{2+}.[20] Moreover, in the case of erbium doping there is need for charge compensation, such as a positive ion vacancy, for each Er^{3+} ion. The error bars shown in Fig. 4 for the lifetime measurements of the 630-nm bands are large because of the much greater intensity of the 582-nm band (and its long lifetime) at temperatures below 40 K. Above this temperature, of course, the 582-nm band has disappeared and the error bars are much less.

The data shown in Figs. 3 and 4 are similar to the previously published results of Holloway *et al.*[4] and Gooen *et al.*[8] for undoped material. The minor difference between the data presented here and that of Gooen *et al.*[8] for the temperature dependence of the lifetime for the 582-nm emission is most likely due to sample variation rather than to measurement error.[20,33] The temperature dependence of the lifetime of the 582-nm emission can be fit with an "activation-type" expression of the form

$$1/\tau = 1/\tau_0 + (1/\tau_{NR})e^{-\Delta/kT}. \quad (1)$$

In this case τ_{NR} is the nonradiative lifetime, Δ is an activation energy, and τ_0 is assumed to be the radiative lifetime. A summary of these parameters is given in Table II together with those from other crystal systems.[19,20,23,34,35]

Several peripheral experimental observations may be of interest. The sharp line structure on the high energy side of the 630-nm band for both

TABLE II. Lifetime fitting parameters for the temperature dependence of the impurity-perturbed Mn^{2+} emission in similar crystals.

Material	τ_0 (msec)	τ_{NR} (msec)	Δ (cm^{-1})
$RbMnF_3$	63	4×10^{-5}	227
$RbMnF_3$ (Ref. 8)	55	10^{-6}	300
$RbMnF_3$:Er^{3+}	49	1.68×10^{-6}	320
MnF_2 (Ref. 23)	38	2.5×10^{-5}	250
MnF_2:Er^{3+} (Ref. 23)	34	10^{-3}	250
$KMnF_3$ (Ref. 19, 34)	60		
$RbMg_xMn_{1-x}F_3$ (Ref. 20)			
$X=0.3$	47	10^{-3}	285
$X=0.6$	33	5×10^{-3}	304

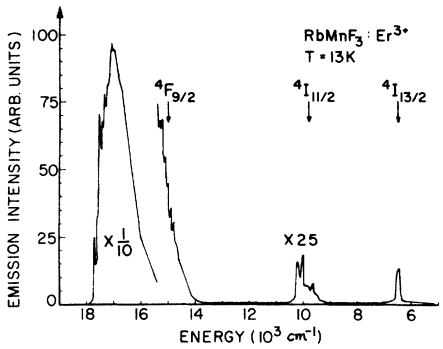

FIG. 5. Low-temperature emission spectra for $RbMnF_3$:Er^{3+}. The broadband and the associated high-energy lines can be attributed, respectively, to impurity perturbed Mn^{2+} and their associated zero phonon lines. The emissions at 15 000, 9813, and 6464 cm^{-1} are due to Er^{3+}. No emission was observed from either the $^4S_{3/2}$ or the $^4I_{9/2}$ levels of Er^{3+}. The curve has been corrected for spectral response and the relative intensities of the different bands may be compared.

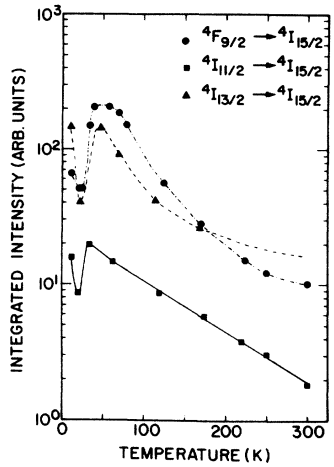

FIG. 7. Temperature dependence of the integrated emission intensity for each of the observed Er^{3+} transitions in Fig. 5. The relative intensities may be different (±50%) than shown because of interfering Mn^{2+} emission and the temperature dependence of lifetime.

the doped and undoped material is different than that for the 582-nm emission. There are differences also between the doped and undoped specimens in the sharp line sequences. It was observed that the intensity of the Mn^{2+} emission takes a time t_{max} to reach a maximum before decaying and for the temperature range of 25–30 K our observations agreed with those reported by Gooen *et al.*[8]

B. Er^{3+} emission

The low-temperature emission spectrum for $RbMnF_3$:Er^{3+} is shown in Fig. 5. The intense emission in the high-energy region of the spectrum is due to Mn^{2+}. The sharp lines are mostly impurity-perturbed zero phonon lines.[7] On the low-energy side of the Mn^{2+} emission, near 15 000 cm^{-1}, the $^4F_{9/2} \rightarrow {}^4I_{15/2}$ emission for Er^{3+} is shown. The groups of lines in the 9813 and 6464 cm^{-1} regions are transitions from the $^4I_{11/2}$ and $^4I_{13/2}$ levels of Er^{3+} to the ground state. Henceforth we will refer to these Er^{3+} transitions under the arrows in Fig. 5 by the level from which they originate.

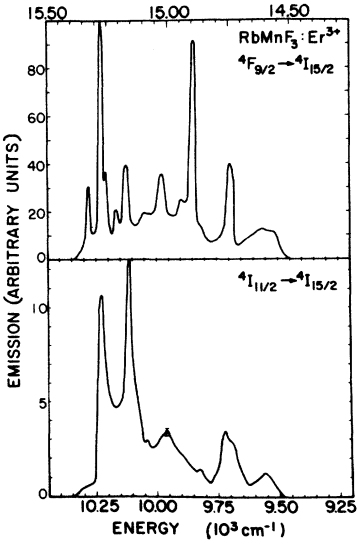

FIG. 6. Expanded view of the $^4F_{9/2} \rightarrow {}^4I_{15/2}$ and $^4I_{11/2} \rightarrow {}^4I_{15/2}$ emissions in $RbMnF_3$:Er^{3+} at $T \sim 13$ K.

In Fig. 6 an expanded view of $^4F_{9/2}$ and $^4I_{11/2}$ luminescence is shown. Since the Mn^{2+} lifetime is very long at low temperatures, the Mn^{2+} background was subtracted from the $^4F_{9/2}$ emission by placing a 450-*Hz* chopper in the exciting light. Integration of the emission intensity of Er^{3+} results in a plot of the temperature dependence of the intensity as shown in Fig. 7. The rise in Er^{3+} intensity occurs in the same temperature region that the Mn^{2+} intensity decreases. This suggests energy transfer from $Mn^{2+} \rightarrow Er^{3+}$. For each of the three Er^{3+} transitions shown a different detector was used to obtain the integrated intensity. An estimate of the relative intensities was made by comparing the $^4F_{9/2}$ and $^4I_{11/2}$ emissions with an RCA7102 photomultiplier tube. The $^4I_{11/2}$ and $^4I_{13/2}$ emissions were compared with a PbS cell. The relative intensities may be different ±50% because of interferring Mn^{2+} emission and the temperature dependence of lifetime.

In Fig. 8 low-temperature excitation spectra are shown for Mn^{2+} and the $^4F_{9/2}$ Er^{3+} emissions (see Fig. 5). The similarity of the manganese excitation spectrum (dashed line) with the Er^{3+} excitation spectrum (solid line) indicates that

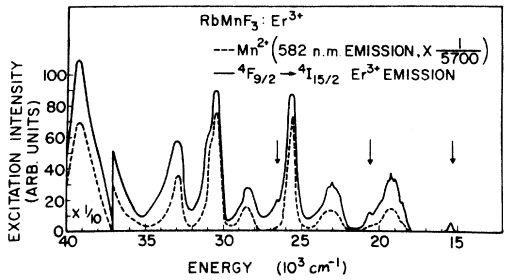

FIG. 8. Excitation spectrum for the $^4F_{9/2}Er^{3+}$ emission shown in Fig. 5. The $^4F_{9/2}$ excitation spectrum is similar to the Mn^{2+} absorption (excitation) spectrum but there are several additional bands due to direct excitation of the Er^{3+}. At 40 K the Mn^{2+} excitation bands increase in intensity while the direct Er^{3+} excitation bands remain relatively constant. This spectrum has been corrected for spectral response.

there is $Mn^{2+} \rightarrow Er^{3+}$ energy transfer. In addition to the broad Mn^{2+} excitation bands, several sharp lines are observed. These are due to direct excitation of the erbium and are emphasized by arrows. As the temperature is raised to 40 K, the excitation bands due to Mn^{2+} increase in intensity while the $^4F_{9/2}Er^{3+}$ excitation band remains relatively constant. As the temperature is increased to 300 K the manganese bands decrease in intensity but are still clearly distinguishable. Similar behavior was found for the $^4I_{11/2}$ and $^4I_{13/2}Er^{3+}$ emissions.

From the overlap of the Mn^{2+} emission with the $^4F_{9/2}$ band shown in Fig. 5, it is clear that any attempt to measure the lifetime of the $^4F_{9/2}$ should be a sum of at least two exponentials. Fortunately, below 120 K the Mn^{2+} emission has a much longer lifetime than $^4F_{9/2}$. This allows for an easy separation. Above 140 K, the Mn^{2+} emission intensity and lifetime have decreased sufficiently to be no longer a problem. A single exponential decay is found for the $^4F_{9/2}$ portion of the total decay. The temperature dependence of the lifetimes for the three Er^{3+} luminescence transitions is depicted in Fig. 9.

As can be seen from Fig. 1, energy transfer from Mn^{2+} ions can populate the $^4F_{9/2}$ level of Er^{3+}, resulting in emission. It is clear also that nonradiative transitions from $^4F_{9/2}$ to $^4I_{9/2}$ and subsequently to $^4I_{11/2}$ and $^4I_{13/2}$ take place. This means that both the $^4I_{11/2}$ and $^4I_{13/2}$ emissions can increase in intensity as a function of time before decaying because of the nonradiative transitions from the upper levels. This type of decay is often called "fluorescent rise type" of decay.[24] A fluorescent rise type of decay was not observed for the $^4I_{11/2}$ emission on the time scales used to measure the single exponential decay. However, the

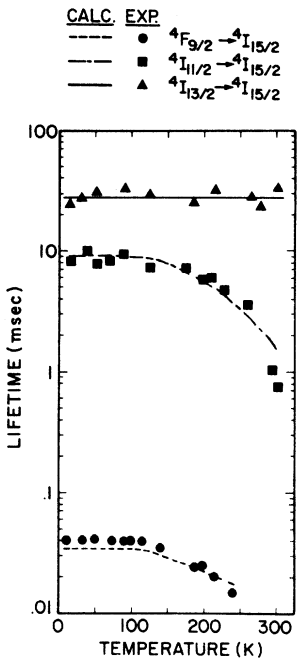

FIG. 9. Temperature dependence of the lifetimes for the Er^{3+} emission bands. The lines correspond to the lifetimes predicted by the theory of Struck and Fonger (Ref. 26). The parameters used for the $^4F_{9/2} \rightarrow {}^4I_{15/2}$ and the $^4I_{11/2} \rightarrow {}^4I_{15/2}$ transitions are summarized in Tables III and IV.

$^4I_{13/2}$ emission was found to be the fluorescent rise type of decay. As the temperature increased the time (t_{max}) to reach the maximum intensity decreased. This behavior of the $^4I_{13/2}$ emission is illustrated in Fig. 10.

IV. DISCUSSION

A. Manganese emission

It has been shown that MnF_2 contains a few ppm of impurities such as Ca, Zn, and Mg.[7] This is

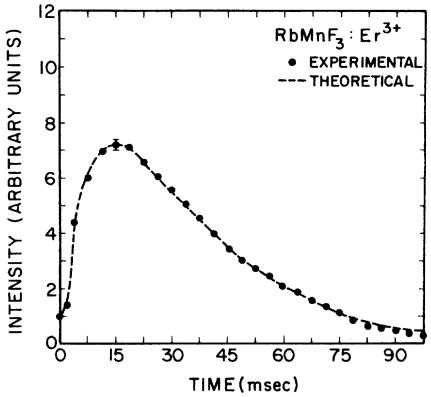

FIG. 10. Emission intensity from the $^4I_{13/2}$ level of Er^{3+} in $RbMnF_3$ at $T = 33$ K as a function of time. The points are experimental and the curve a theoretical fit.

most likely also the case for $RbMnF_3$. Distinct zero phonon lines are associated with each type of impurity for the perturbed Mn^{2+} emission at 582-nm.[7,18] It is not known at this time what type of defect or impurity is responsible for the perturbed Mn^{2+} emission at 630-nm. Since the excitation spectra of these bands are the same and are identical with the Mn^{2+} intrinsic absorption it is clear that energy transfer occurs from unperturbed ions, which have very long lifetimes, to the perturbed ions. As the sample temperature is increased, energy transfer is enhanced. The fitting of the temperature dependence of the lifetime of the 582-nm emission by an activation type curve [Eq. (1)] with Δ as an activation energy is possible, but the existence of different values of Δ for the various crystals suggests that the levels are perturbed by impurities and/or mechanical strain.

B. Erbium emission

When an Er^{3+} ion substitutes for a Mn^{2+} ion in $RbMnF_3$ it has O_h symmetry unless the charge compensating defect is close by. If O_h symmetry is assumed, then the crystal field should split the $^4F_{9/2}$ level into three levels, the $^4I_{11/2}$ level into four, and the $^4I_{13/2}$ and $^4I_{15/2}$ into five levels each.[35] This indicates that the ground state should have at least five levels upon which emission from an excited state can terminate. In Fig. 6 the emission from the $^4F_{9/2}$ and $^4I_{11/2}$ excited states have been aligned to determine if bands can be detected in both which agree and may be due to transitions to the ground state levels. Although these emission bands are very similar to those reported earlier[24] it is expected that the ground state levels will be split by less than 300 cm^{-1}.[36,37] The extent of the spectra shown in Fig. 6 is 750 cm^{-1}. The excited state levels have very small splittings and thermal population of these levels is possible.[32,36,37] This complicates the picture considerably. For example, the temperature dependence of the major peaks in Fig. 6 differ and although there is a suggestion that bands with energy separations of 150, 300, 550, and 700 cm^{-1} are related to the same transitions, it is not possible to be certain.

C. $Mn^{2+} \rightarrow Er^{3+}$ energy transfer

The best evidence for $Mn^{2+} \rightarrow Er^{3+}$ energy transfer is shown in Fig. 8 by the presence of manganese bands in the Er^{3+} excitation spectra. Direct excitation of the Er^{3+} absorption bands is noted but most of the emission is a result of $Mn^{2+} \rightarrow Er^{3+}$ energy transfer. The fact that the Mn^{2+} excitation bands can be seen in the Er^{3+} excitation spectrum at room temperature suggests that the energy-transfer process is nonradiative. Additional evidence for this nonradiative energy transfer is found by comparing the decrease in manganese emission intensity between 10–50 K with a corresponding increase in the Er^{3+} intensity in the same temperature region. This is contrary to expected behavior for radiative energy transfer. Moreover, this increase of the Er^{3+} emission with temperature corresponds to the same temperature region in which repopulation of the intrinsic Mn^{2+} band from the 582-nm level occurs.

The model of Flaherty and Di Bartolo[23] with some modifications can be used to help explain these observations. It is possible that at very low temperatures the Mn^{2+} "exciton" is free to move through the lattice. As the temperature is raised to 20-K exciton-phonon interactions decrease the number of excitons available to interact with the Er^{3+}. This is evidenced by an initial decrease in the intensity of the Er^{3+} emission and a slight decrease in the impurity-perturbed manganese emission. At 40 K the 582-nm band is thermally repopulating the number of available excitons so that the Er^{3+} emission increases. As the temperature is raised further exciton-phonon interactions and Er^{3+}-phonon interactions become increasingly competitive. The result is a decrease in the Er^{3+} emission. Clearly this suggested model warrants further experimental investigation.

D. Radiative and nonradiative relaxation of Er^{3+} in $RbMnF_3$

Over the years a number of different techniques[31,32,38-40] have been developed to determine multiphonon rates. Independent of the above techniques which require either an absolute measurement or calculation of the radiative rate, Struck and Fonger[26-30] have developed a quantum-mechanical single-configuration-coordinate model which can explain the temperature dependence of lifetimes. When absorption, emission and lifetime data are available a prediction of the temperature dependence of the nonradiative rate can be made and a reasonable configuration coordinate diagram can be constructed using the available data and the Struck and Fonger analysis. This will allow a determination of the nonradiative rates. The model will be checked by an independent calculation of the nonradiative rate using the model of Flaherty and Di Bartolo[24] which requires lifetimes and integrated intensities at two different temperatures for two levels.

The QMSCC model of Struck and Fonger predicts the temperature quenching of the lifetime from the seven following experimentally related parameters: $\hbar\omega$ is the interacting phonon energy, p_U is the

number of these phonons emitted over the energy gap of interest, T is the temperature, a_{uv} is the relative offset of the two parabolas in the configuration-coordinate curve, θ which is related to the ratio of the interacting phonon frequencies of the two levels, and finally, N_{uv} and R_{uv} which are the nonradiative and radiative electronic factors. A simplified flowchart to calculate the temperature quenching of the lifetime has been described elsewhere.[41] Basically p_U and θ are inserted into the Mannebach recursion relations[26] to calculate the overlap integrals ($\langle u_n | v_m \rangle$) of the nth harmonic oscillator wave function of the u parabola with respect to the mth harmonic oscillator wave function of the v parabola. The radiative and nonradiative rates ($R_{p_U v}$ and $N_{p_U v}$) are related to these overlap integrals through the U_{p_U} term in following expressions:

$$N_{p_U v} = N_{uv} U_{p_U}, \quad R_{p_U v} = R_{uv} U_{p_U}, \tag{2}$$

which are partially governed by their respective energy balances for the transition

$$\begin{aligned} h\nu_{zp,\,uu} - p_u \hbar\omega_u + h\nu_{p_U} &= 0, \\ h\nu_{zp,\,uu} - p_u \hbar\omega_u &= 0. \end{aligned} \tag{3}$$

Here $h\nu_{zp,\,uu}$ refers to the zero-phonon energy, while $h\nu_{p_U}$ refers to photon energy of all unresolved radiative transitions with quantum number p_U. These energy balances together with θ select particular overlap matrix elements for calculation of U_{p_U} in the following expression[26]:

$$U_{p_U} = \sum_{m=0}^{\infty} (1 - r_v) r_v^m [f_m \langle u_{p_U + i_m - 1} | v_m \rangle^2 + (1 - f_m) \langle u_{p_U + i_m} | v_m \rangle^2] \quad \text{for } p_U \geq 0. \tag{4}$$

Note first that the term outside the square brackets predicts the temperature dependence of the rate through the Boltzmann factor [$r_v = \exp(-\hbar\omega_v / kT)$]. The remaining undefined variables are as follows: i_m is the smallest integer $\geq (\hbar\omega_v / \hbar\omega_u)m$ and $f_m = i_m - (\hbar\omega_v / \hbar\omega_u)m = i_m - (\tan^2\theta)m$. Second, note that for $\theta = 45°$, $\hbar\omega_v = \hbar\omega_u$, and $f_m = 0$. This means in the equal force constant case ($\theta = 45°$)

$$U_{p_U}(45°) = W_{p_U} = \sum_{m=0}^{\infty} (1 - r_v) r_v^m \langle u_{p_U + m} | v_m \rangle^2 \quad \text{for } p_U \geq 0. \tag{5}$$

Thus for p_U equal to 14, the sum would start on the fourteenth row down with $m = 0$ and then progressively down a diagonal (i.e., $\langle u_{15} | v_1 \rangle^2$, $\langle u_{16} | v_2 \rangle^2$, etc.). Using trial data these matrix elements squared and their sums reproduced the tables presented in Refs. 26 and 28. For comparison with experiment the following expression was used[26]:

$$1/\tau = R_{uv} + N_{uv} U_{p_U}, \tag{6}$$

where $R_{uv} = 1/\tau_0$ is the low-temperature radiative lifetime. An experimental estimate of N_{uv} can be obtained from the compliance constants measured for $RbMnF_3$ at 4.2 K.[42] A maximum value for N_{uv} was found to be 1.3×10^{13} sec^{-1}. For these calculations a N_{uv} of 1×10^{13} sec^{-1} was used for all cases. An analysis of the temperature dependence of the $^4I_{13/2}$ lifetime can now be made.

Since Er^{3+} is shielded by the 5s and 5p orbitals, a first approach to constructing a configuration coordinate diagram is to assume $\theta = 45°$, i.e., all the levels have the same interacting phonon frequency. An interacting phonon frequency of 267 cm^{-1} was used. This number is in good agreement with the infrared reflectivity data of Perry and Young.[43] From the absorption and emission peaks a_{uv} is found to be 0.38. From the zero phonon energy p_U is approximately 24, thus taking $p_U = 24$, $a_{uv} = 0.38$, $\hbar\omega_v = 267$ cm^{-1}, $\theta = 45°$, and $N_{uv} = 1 \times 10^{13}$ sec^{-1} a temperature-independent lifetime was found as evidenced by the straight line in Fig. 9. These data can also be used along with an effective mass of six fluorines to construct a configuration coordinate diagram as shown in Fig. 11 where it can be seen that the $^4I_{13/2}$ parabola does not cross the ground-state parabola.

Next we consider the $^4I_{11/2}$ level which has nonradiative decay only to the $^4I_{13/2}$ level. Clearly, p_U will be smaller in this case due to the smaller energy gap. The best obtained fit is illustrated by

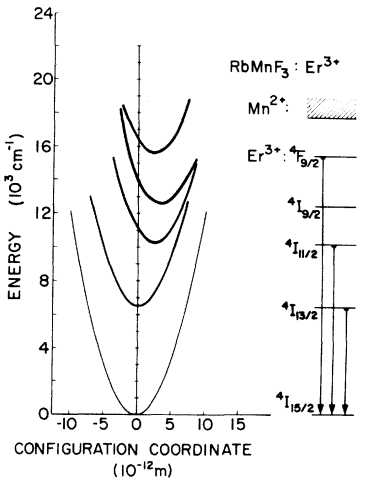

FIG. 11. Configuration coordinate diagram for the lower levels of Er^{3+} in $RbMnF_3$. This figure can be used to show the energy of absorption bands in Fig. 1, the emission band energies in Fig. 5 and finally the temperature quenching of the lifetime shown in Fig. 9. An energy-level diagram with the three observed transitions is shown on the right.

TABLE III. Results obtained using Struck and Fonger's matrix method for the $^4I_{11/2} \rightarrow {}^4I_{15/2}$ emission of Er^{3+} in $RbMnF_3$. The parameters used are as follows: $p_U = 14$, $a_{uv} = 1.9$, $\hbar\omega_v = 267$ cm^{-1}, $\theta = 45°$, and $N_{uv} = 1 \times 10^{13}$ sec^{-1}.

T (K)	$10^{-12}U_{p_U}$	$\langle m \rangle_{p_U}$	$\langle m \rangle_v$	E_{p_U} (cm^{-1})	A_{p_U} (sec^{-1})	τ_{expt} (msec)	τ_{calc} (msec)
15	1.11	9.4×10^{-12}	7.1×10^{-12}	2.31×10^{-8}	19.1	8.4	9
40	1.11	8.8×10^{-4}	6.6×10^{-5}	0.214	19.23	10	9
52	1.12	8.1×10^{-3}	6.1×10^{-4}	1.97	20.3	7.9	9
70	1.16	0.054	4.1×10^{-3}	13.3	26.4	8.3	9
87	1.28	0.16	0.012	39.2	42.4	9.7	8.9
125	1.97	0.63	0.048	155.5	2.03	7.5	8.4
175	4.61	1.63	0.125	397	2×10^3	7.3	6.8
200	7.48	2.22	0.17	541	6.3×10^3	6.0	5.7
210	9.11	2.46	0.19	602	9.1×10^3	6.1	5.2
236	15.29	3.13	0.243	763.8	2.7×10^4	5.15	4
247	19.03	3.42	0.266	834	4.2×10^4	5.4	3.4
260	24.62	3.76	0.294	917	6.8×10^4	3.7	2.9
278	35.06	4.24	0.334	1035.4	1.3×10^5	1	2.2
297	52.57	4.81	0.381	1173.4	2.5×10^5	0.75	1.6

the broken line in Fig. 9. Actual experimental and theoretical values together with other parameters such as $U_{p_U}\langle m \rangle_{p_U}$, $\langle m \rangle_v$, E_{p_U}(cm^{-1}), and A_{p_U} are given in Table III. a_{uv} in this "best" fit case is the relative displacement of the $^4I_{11/2}$ parabola with respect to the $^4I_{13/2}$ parabola. Again from absorption and emission peak positions an absolute displacement between the $^4I_{11/2}$ parabola and the ground state parabola of 2.3 can be determined. This is approximately the sum of 0.38 and 1.9.

For the case of the temperature quenching of the lifetime for the $^4F_{9/2}$ emission it is assumed that the $^4F_{9/2}$ nonradiatively feeds only the $^4I_{9/2}$. The best fit for the QMSCC model to the data is illustrated by the dashed line in Fig. 9. A summary of the various parameters is given in Table IV. An a_{uv} of 1.49 represents the relative displacement of the $^4F_{9/2}$ parabola from the $^4I_{9/2}$ parabola. From absorption and emission measurements the absolute displacement of the $^4F_{9/2}$ parabola is 1.93. Looking at the ^4I_J paraboli constructed so far it seems physically reasonable that for increasing J the parabola's should be increasingly offset from zero. With this in mind the absolute displacement of the $^4I_{9/2}$ can be estimated as $1.93 + 1.49 = 3.42$. The displacement of the $^4I_{11/2}$ was found previously to be 2.28. Thus the following parameters should be inserted into the Struck and Fonger matrix method to predict the nonradiative rate between $^4I_{9/2}$ and $^4I_{11/2}$: $\theta = 45°$, $a_{uv} = 3.42 - 2.28 = 1.14$, $p_U = 8$, $\hbar\omega_v = 267$, and $N_{uv} = 1 \times 10^3$ sec^{-1}. The results predicted from these parameters are given in Table V.

The nonradiative rate for the levels at low temperatures can now be plotted versus the energy gap between these different levels. This is shown in Fig. 12. Note that the predicted nonradiative rate between $^4I_{9/2}$ and $^4I_{11/2}$ lies very close to the line drawn through the rates for $^4F_{9/2}$ and $^4I_{11/2}$. Thus, the Struck and Fonger matrix method predicts an experimentally reasonable energy gap law dependence. Energy gap parameters and phonon

TABLE IV. Results obtained using Struck and Fonger's matrix method for the $^4F_{9/2} \rightarrow {}^4I_{15/2}$ emission of Er^{3+} in $RbMnF_3$. The parameters used are as follows: $p_U = 10$, $a_{uv} = 1.49$, $\hbar\omega_v = 267$ cm^{-1}, $\theta = 45°$, and $N_{uv} = 1 \times 10^{13}$ sec^{-1}.

T (K)	$10^{-9}U_{p_U}$	$\langle m \rangle_{p_U}$	$\langle m \rangle_v$	E_{p_U} (cm^{-1})	A_{p_U} (10^3 sec^{-1})	τ_{expt}(μsec)	τ_{calc} (μsec)
13	0.44	1.36×10^{-12}	1.37×10^{-13}	3.27×10^{-10}	4.38	39.6	34.4
50	0.44	4.5×10^{-3}	4.53×10^{-4}	1.07	4.54	40.5	34.4
72	0.46	0.047	4.8×10^{-3}	11.4	5.75	40.5	34.4
100	0.53	0.215	0.022	51.6	11.1	40.0	33.3
116	0.61	0.37	0.037	88.96	18.4	39.7	32.4
140	0.79	0.67	0.068	161.3	41.5	35.0	30.7
187	1.46	1.43	0.146	341	205	24.5	25.4
197	1.69	1.61	0.165	385	284	25	24.0
215	2.19	1.95	0.2	466	500	20	21.4
240	3.16	2.43	0.25	581	1044	15.0	17.7

TABLE V. Results obtained using Struck and Fonger's matrix method for the $^4I_{9/2}$ and $^4I_{11/2}$ levels of Er^{3+} in $RbMnF_3$. The parameters used are as follows: $p_U = 8$, $a_{uv} = 1.14$, $\hbar\omega = 267$ cm^{-1}, $\theta = 45°$, and $N_{uv} = 1\times10^{13}$ sec^{-1}.

T (K)	$10^{-9}U_{pU}$	$<m>_{pU}$	$<m>_v$	E_{pU} (cm^{-1})	A_{pU} (10^4 sec^{-1})	$N_{uv}U_{pU}$ (10^4 sec^{-1})
15	2.23	5.96×10^{-11}	7.13×10^{-12}	1.39×10^{-8}	2.22	2.23
40	2.23	5.52×10^{-4}	6.6×10^{-5}	0.12	2.23	2.23
52	2.24	5.1×10^{-3}	6.1×10^{-4}	1.2	2.31	2.24
70	2.29	0.03	4.1×10^{-3}	8	2.7	2.29
87	2.43	0.1	0.01	23.7	3.6	2.43
125	3.14	0.4	0.05	94	9.3	3.14
175	5.26	1	0.12	242	38.7	5.26
200	7.05	1.4	0.17	330	76.6	7.05
210	7.95	1.6	0.19	368	99.5	7.95
236	10.88	2.0	0.24	468	190	10.88
247	12.44	2.2	0.26	512	247	12.44
260	14.55	2.4	0.29	564	333	14.55
278	18.05	2.7	0.33	638	500	18.05
299	23.14	3.1	0.38	725	770	23.14

coupling parameters are summarized for several materials containing Er^{3+} in Table VI.

Now that a configuration coordinate diagram (Fig. 11) has been constructed it should be pointed out that the lack of emission from the $^4I_{9/2}$ level can be explained by the relatively low intersection of $^4I_{9/2}$ with $^4I_{11/2}$. This is consistent with the high nonradiative rates in Table V.

As mentioned earlier Flaherty and Di Bartolo[24] have developed an expression to determine the

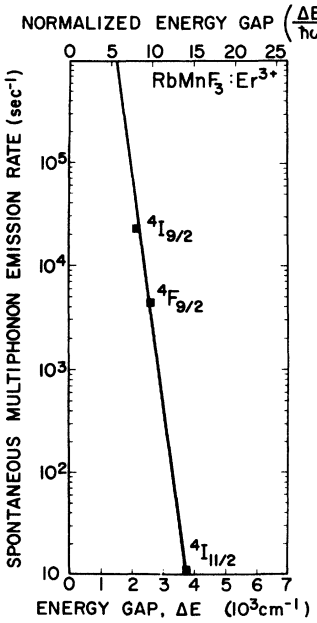

FIG. 12. Spontaneous multiphonon transition rate versus gap energy of Er^{3+} in $RbMnF_3$. The fitting parameters for the line shown are given in Table VI. The data points were taken from the values for the product $N_{uv}U_{pu}$ at 15 K in Tables III, IV, and V.

nonradiative transition rate between two levels A and B. It seems prudent to compare their method with the QMSCC model. The time dependence of the rise in $^4I_{13/2}$ intensity is controlled by the nonradiative rate p_{AB} between the $^4I_{11/2}(A)$ and $^4I_{13/2}(B)$ parabolas and the lifetime of the $^4I_{11/2}$. Using the two rate equations

$$\frac{dn_A}{dt} = -n_A(p_A + p_{AB}) \approx -n_A p_A \tag{7}$$

and

$$\frac{dn_B}{dt} = n_A p_{AB} - n_B p_B , \tag{8}$$

Flaherty and Di Bartolo[24] developed the following expression for the time dependence of the $^4I_{13/2}$ emission:

$$\frac{n_B(t)}{n_B(0)} = \left(1 + \frac{n_A(0)}{n_B(0)}\frac{p_{AB}}{p_A - p_B}\right)e^{-p_B t} - \frac{n_A(0)}{n_B(0)}\left(\frac{p_{AB}}{p_A - p_B}\right)e^{-p_A t} , \tag{9}$$

where

$$p_A = 1/\tau_A \quad \text{and} \quad p_B = 1/\tau_B .$$

Equation (9) can be derived by taking the Laplace

TABLE VI. Energy-gap law parameters for several materials containing erbium.

Material	C (sec^{-1})	α (cm)	ϵ
$RbMnF_3:Er^{3+}$	1.06×10^9	4.7×10^{-3}	0.179
$MnF_2:Er^{3+}$ (Ref. 25)	5.5×10^7	4.3×10^{-3}	0.259
$Y_2O_3:Er^{3+}$ (Ref. 34)	2.7×10^8	3.8×10^{-3}	0.12

transform of Eqs. (7) and (8) and expanding in partial fractions. At low temperatures p_{AB} can be estimated from the Struck and Fonger calculation to be 11.1 sec^{-1}. At 33 K, $p_A = 111$ sec^{-1} and $p_B = 35.7$ sec^{-1}. Substituting these values into Eq. (8) it is seen in Fig. 10 that the theory matches the experimental data. By setting the derivative of Eq. (9) to zero, the time (t_{max}) the intensity takes to reach a maximum can be calculated by the following formula[24]:

$$t_{max} = \frac{1}{p_B - p_A} \ln\left(\frac{p_B}{p_A} + \frac{p_B(p_A - p_B)}{p_A p_{AB}} \frac{n_B(0)}{n_A(0)}\right). \quad (10)$$

Substituting the values given above and determining $n_B(0)/n_A(0)$ by normalization of Eq. (9) to experiment, a value of 13.2 msec can be found. As the temperature increases, t_{max} decreases consistent with the increase in the nonradiative rate p_{AB}.

Flaherty and Di Bartolo[24] also have developed an expression for the nonradiative rate between two levels A and B using only lifetimes and integrated intensities of these levels at two different temperatures. Let level A be the $^4F_{9/2}$ level and level B be $^4I_{11/2}$. Experimentally, emission is observed from levels A and B but not from the intermediate $^4I_{9/2}$. This means that the nonradiative rate should be much more than the radiative rate from $^4I_{9/2}$. In other words, all ions excited into the $^4I_{9/2}$ state should decay into $^4I_{11/2}$. Thus, the nonradiative rate between level A and B predicted by Flaherty and Di Bartolo should reflect the rate between the $^4F_{9/2}$ and $^4I_{9/2}$ levels. The expression developed by Flaherty and Di Bartolo is as follows:

$$p_{AB}(T_2) = \left(\frac{1}{\tau_A(T_2)} - \frac{1}{\tau_A(T_1)}\right) \times \left\{1 - \frac{\tau_B(T_2)}{\tau_B(T_1)}\left[\left(\frac{I_A(T_2)}{I_B(T_2)}\right)\left(\frac{I_B(T_1)}{I_A(T_1)}\right)\right]\right\}^{-1}. \quad (11)$$

For $T_1 = 184$ K, we have $\tau_A(T_1) = 0.027$ msec, $\tau_B(T_1) = 6.5$ msec, and $I_B(T_1)/I_A(T_1) = 2.05$. In the case of $T_2 = 222$ K, we have $\tau_A(T_2) = 0.02$ msec, $\tau_B(T_2) = 5.4$ msec, and $I_B(T_2)/I_A(T_2) = 0.25$. From these values p_{AB} is found to be 2.26×10^4 sec^{-1}. From Table IV, $p_{SF} = N_{uv}U_{p_U}$ at 215 K is 2.19×10^4 sec^{-1} which is in reasonable agreement. The nonradiative rates p_{AB} and p_{SF} may be compared absolutely at two temperatures[24] by the following expressions:

$$\frac{p_{AB}(T_2)}{p_{AB}(T_1)} = \frac{\tau_B(T_1)}{\tau_B(T_2)}\left[\left(\frac{I_A(T_1)}{I_B(T_1)}\right)\left(\frac{I_B(T_2)}{I_A(T_2)}\right)\right], \quad (12)$$

$$\frac{p_{SF}(T_2)}{p_{SF}(T_1)} = \frac{N_{uv}U_{p_U}(T_2)}{N_{uv}U_{p_U}(T_1)} = \frac{U_{p_u}(T_2)}{U_{p_u}(T_1)}. \quad (13)$$

Again from Table IV at 215 K $p_{SF}(184) = 1.45 \times 10^4$ sec^{-1}. Substituting the numbers into Eqs. (13) and (12),

$$U_{p_U}(T_2) / U_{p_U}(T_1) = 1.72,$$

while

$$p_{AB}(T_2)/p_{AB}(T_1) = 2.34.$$

Thus the configuration-coordinate model predicted by the use of Struck and Fonger is within 25% of the Flaherty and Di Bartolo calculation. It would be possible to match the two calculations exactly by choosing a lower N_{uv} value for the Struck and Fonger model.

V. CONCLUSIONS

(i) A small effect due to the presence of Er^{3+} on the Mn^{2+} emission was noted when the temperature dependence of the lifetimes was compared for $RbMnF_3$ and $RbMnF_3$:Er^{3+}.

(ii) No emission was observed from the $^4I_{9/2}$ or $^4S_{3/2}$ levels of Er^{3+} in $RbMnF_3$.

(iii) The temperature dependence of the emission integrated intensity and excitation spectra indicated nonradiative $Mn^{2+} \rightarrow Er^{3+}$ energy transfer.

(iv) The $^4I_{13/2} \rightarrow {}^4I_{15/2}$ and $^4I_{11/2} \rightarrow {}^4I_{15/2}$ emissions of Er^{3+} were found to have lifetimes between 0.75–35 msec.

(v) The matrix method of Struck and Fonger, together with absorption and emission energies, were used to construct a configuration-coordinate diagram. Nonradiative rates predicted by the Struck and Fonger analysis were compared with intensity versus time data of the $^4I_{13/2}$ and the predictions of the model of Flaherty and Di Bartolo. Good agreement was obtained.

VI. ACKNOWLEDGMENTS

This work was supported by NSF Grant No. DMR 77-12594. One of us (M.V.I.) was a 3M Company Fellow whose support is appreciated. Many helpful discussions with R. C. Powell are also gratefully acknowledged.

[1] D. S. McClure, in *Solid State Physics*, edited by F. Seitz and D. Turnbull (Academic, New York, 1959), Vol. 9, p. 399.

[2] J. F. Sabatini, A. E. Salwin, and D. S. McClure, Phys. Rev. B 11, 3832 (1975).

[3] W. W. Holloway, Jr., M. Kestigan, R. Newman, and E. W. Prohofsky, Phys. Rev. 11, 82 (1963).

[4] W. W. Holloway, Jr., E. W. Prohofsky, and M. Kestigan, Phys. Rev. 139, A954 (1965).

[5] W. W. Holloway, Jr. and M. Kestigan, Phys. Status

Solidi 28, K159 (1969).
[6]A. Mehra and P. Venkateswarlu, J. Chem. Phys. 47 2334 (1967).
[7]R. L. Green, D. D. Sell, R. S. Feigelson, G. F. Imbusch, and H. J. Guggenheim, Phys. Rev. 171, 600 (1968).
[8]K. Gooen, B. Di Bartolo, M. Alam, R. C. Powell, and A. Linz, Phys. Rev. 177, 615 (1969).
[9]J. Ferguson, H. J. Guggenheim, and Y. Tanabe, Phys. Rev. 161, 207 (1967).
[10]J. Ferguson, Aust. J. Chem. 21, 307 (1968).
[11]J. Ferguson, G. Osborne, N. Fuchikami, and Y. Tanabe, J. Phys. Soc. Jpn. 41, 1326 (1976).
[12]V. V. Eremenko, E. V. Matyushin, and S. V. Petrov, Phys. Status Solidi 18, 683 (1966).
[13]E. V. Matyushkin, L. L. Kukushkin, and V. V. Eremenko, Phys. Status Solidi 22, 65 (1967).
[14]V. V. Eremenko and E. V. Matyushkin, Opt. Spektrosk. 23, 437 (1967) [Opt. Spectrosc. (U.S.S.R) 23, 234 (1967)].
[15]E. V. Matyushkin and N. N. Rozhitski, Fiz. Tverd. Tela (Leningrad) 10, 2214 (1968) [Sov. Phys.-Solid State 10, 1736 (1969)].
[16]B. A. Wilson, W. M. Yen, J. Hegarty, and G. F. Imbusch, Phys. Rev. B 19, 4238 (1979).
[17]R. Kumar, Chem. Phys. Lett. 45, 121 (1977).
[18]G. F. Imbusch, in *Luminescence in Inorganic Solids*, edited by B. Di Bartolo (Wiley, New York, 1977), p. 155.
[19]V. Goldberg, V. Moncorge, D. Pacheco, and B. Di Bartolo, in Ref. 18, p. 603.
[20]N. Koumvakalis, W. A. Sibley, and G. F. Venikouas, J. Lumin. 15, 283 (1977).
[21]M. Hirano and S. Shionoya, J. Phys. Soc. Jpn. 28, 926 (1970).
[22]S. Shionoya and M. Hirano, Phys. Lett. 26A, 533 (1968).
[23]J. M. Flaherty and B. Di Bartolo, Phys. Rev. B 8, 5232 (1973).
[24]J. M. Flaherty and B. Di Bartolo, J. Lumin. 8, 51 (1973).
[25]J. M. Flaherty and B. Di Bartolo, Colloq. Int. C. N. R. S. 255, 191 (1977).
[26]C. W. Struck and W. H. Fonger, J. Lumin. 10, 1 (1975).
[27]W. H. Fonger and C. W. Struck, Phys. Rev. B 11, 3251 (1975).
[28]C. W. Struck and W. H. Fonger, J. Lumin. 14, 253 (1976).
[29]W. H. Fonger and C. W. Struck, J. Chem. Phys. 60, 1994 (1974).
[30]W. H. Fonger and C. W. Struck, J. Lumin. 17, 241 (1978).
[31]M. J. Weber, in *Optical Properties of Ions in Crystals*, edited by H. M. Crosswhite and H. W. Moos (Interscience, New York, 1966).
[32]M. J. Weber, Phys. Rev. 157, 262 (1961).
[33]R. C. Powell (private communication). The authors would also like to thank J. J. Martin, L. E. Halliburton, and N. Koumvakalis for many helpful discussions.
[34]V. Goldberg, D. Pacheco, R. Moncorge, and B. Di-Bartolo, J. Lumin. 18, 143 (1979).
[35]B. Di Bartolo, *Optical Interactions of Ions in Solids* (Wiley, New York, 1968), p. 204.
[36]S. M. Kulpa, J. Phys. Chem. Solids 36, 1317 (1975).
[37]M. V. Petrov and A. M. Tkachuk, Opt. Spektrosk. 45, 147 (1978) [Opt. Spectrosc. (USSR) 45, 81 (1978)].
[38]J. R. Chamberlain, D. H. Paxman, and J. L. Page, Proc. Phys. Soc. London 89, 143 (1966).
[39]L. A. Risberg and M. J. Weber, in *Progress in Optics*, edited by E. Wolf (Elsevier, New York, and North-Holland, Amsterdam, 1977), Vol. XIV, p. 89.
[40]W. D. Partlow and H. W. Moos, Phys. Rev. 157, 252 (1967).
[41]M. V. Iverson, Ph.D. thesis, Oklahoma State University, 1979 (unpublished).
[42]R. L. Melcher and D. I. Bolef, Phys. Rev. 178, 864 (1969).
[43]C. M. Perry and E. F. Young, J. Appl. Phys. 38, 4616 (1967); 38, 4624 (1967).